# Determination of the Mechanoelastic Properties of Parasites via Analysis of Their Microscopic Images

D. Arabadjis, P. Rousopoulos, C. Papaodysseus, M. Panagopoulos, P. Loumou and G. Theodoropoulos

*Abstract*— **A novel methodology is introduced here that exploits microscopic images of domestic animals' parasites in arbitrary deformation instances, so as to verify assumptions about their mechanoelastic properties. The obtained knowledge of these properties manifests parasite body characteristics that are deformation invariant, thus allowing for unwrapping them. Next, we have stated differential equations that govern the parasite body deformation and we have solved them by performing a set of equivalent image operations on the deformed body images. This process furnishes the parasite undeformed version from its deformed image. The method has been applied to a dataset of 193 microscopic images of highly deformed parasites. It is demonstrated that different orientations and deformations of the same parasite give rise to practically the same undeformed shape, thus confirming the consistency of the approach.**

## I. Introduction

THERE are numerous applications, where bodies suffer deformation due to elastic forces (stresses). In these cases, one frequently encounters to important problems: a) to make consistent and reliable estimation of the deformed bodies' mechano-elastic properties from images of random instances of body deformation and b) to identify the deformed body automatically from these very images. We would like to emphasize that, as a rule, automatic classification of bodies on the basis of images of their deformation, is practically prohibited by the randomness of the deformation. One encounters such problems in various disciplines applications, such as automatic identification of highly deformed parasites, cells or large molecules from their images obtained via microscope, in strength of materials, elastography [1], in civil engineering in general, etc.

In the present paper, we have applied the following new approach to tackle the aforementioned problems as follows: We estimate the mechano-elastic properties of a body suffering an equivalent to 2D deformation from an image of it at an arbitrary deformation instance. Knowledge of these mechano-elastic properties allows for unwrapping/straighten the deformed body image, a fact that in turn permits application of pattern recognition techniques for the body automatic classification/identification. We have applied the introduced to an important and some times crucial veterinary problem, namely the automatic identification of domestic animal parasites, from their images obtained via microscope [2]. These images represent the parasites in a state of serious deformation. Although the introduced approach can be extended so as to be applicable in many 2D bodies deformations, in order to tackle the problems related to parasite bodies more easily, we have made a number of plausible assumptions described in Section II.

D. Arabadjis is with the National Technical University of Athens, e-mail: alphad.d@gmail.com.

P. Rousopoulos is with the National Technical University of Athens, e-mail: panous@ntua.gr.

C. Papaodysseus is with the National Technical University of Athens, phone:+302107722329; fax:+302107640603; e-mail: cpapaod@ cs.ntua.gr.

M. Panagopoulos is with the National Technical University of Athens, e-mail: mpanagop@hotmail.com.

P. Loumou is with the National Technical University of Athens.

G. Theodoropoulos is with the Agricultural University of Athens, e-mail: aanp2thg@noc.aua.gr.

## II. Exploitation of Elasticity Theory for Unwrapping Deformed Objects

### *A. Adopted hypotheses concerning the considered object's elastic properties*

1. All object (e.g. parasite) parts are isotropic, homogeneous and continuous.
2. The static equation of balance holds for the deformed element too (1st order Theory)
3. There exists a curve of symmetry for the undeformed object.
4. Object's straight line segments, the cross sections, which are initially perpendicular to its symmetry curve, remain straight and perpendicular to a proper corresponding line after the deformation, which is usually called neutral line.
5. The cross dimensions are small compared to the symmetry curve's length.
6. The generated stresses and displacements along the object body are linearly related, namely the generalized Hooke's law holds.

The aforementioned hypotheses allow us to study the elastic behavior of the object in two dimensions. Consequently, the information extracted from the deformed object images may be sufficient for this study, for unwrapping the objects and thus obtaining instances useful for their identification.

In the bibliography, there are some approaches for generating the phases between an initial and a final stage of a body elastic deformation [3], [4]. In these publications, images of both the initial and final stages deformation are

available. On the contrary, in the present paper, images of the undeformed body cannot be obtained, hence there are no initial phase representations. Moreover, methods that do not demand given initial body image to perform deformation, use deformable lines or surfaces [5], [6], which are not connected to deformation invariants of body shape. Thus, they cannot be used to create representative undeformed body images from its deformed instances. These facts calls upon an alternative approach which is, for the first time, presented below.

### B. Object body's 2D elastic deformation equations

We assume that the undeformed object has a symmetry curve $M:\ \vec{\mu}(s)=(x_\mu(s),y_\mu(s))$ parameterized via its length s. Then we define the unit vector $\hat{l}(s)=\dot{\vec{\mu}}/\left\|\dot{\vec{\mu}}\right\|$ tangent at an arbitrary point of M at length s and the unit vector $\hat{n}(s)$ normal to $\hat{l}(s)$. Next, coordinates of the points of object's body will be expressed via their distance vector from the symmetry curve $M$. Namely for each point with position vector $x\hat{\imath}+y\hat{\jmath}$ we define the distance vector from object's symmetry line

$$\vec{r}(s,\delta)=\vec{\mu}(s)+\left(x-x_\mu(s)\right)\hat{\imath}+\left(y-y_\mu(s)\right)\hat{\jmath}=\vec{\mu}(s)+\delta\,\hat{n}(s)\ .$$

Thus any differential displacement in the undeformed body is expressed $d\vec{r}(s,\delta)=\left(1+\delta\,\dot{\phi}\right)ds\,\hat{l}(s)+d\delta\,\hat{n}(s)$ where the curvature $\dot{\phi}\,\hat{l}(s)=\dfrac{d}{ds}\hat{n}(s)$. Now, we can represent any differential deformation $du\hat{\imath}+dw\hat{\jmath}$ by using the basis $\left(\hat{l}(s),\hat{n}(s)\right)$ as a curved vector

$$du\,\hat{\imath}+dw\hat{\jmath}=\left(1+\delta_{u,w}\hat{l}^{\,T}(s)\frac{d\hat{n}(s)}{ds_{u,w}}\right)ds_{u,w}\,\hat{l}(t)+d\delta_{u,w}\,\hat{n}(s)$$

$$ds_{u,w}=ds\sqrt{\left(\nabla^T u\,\hat{l}(s)\right)^2+\left(\nabla^T w\,\hat{l}(s)\right)^2}\ ,\ d\delta_{u,w}=d\delta\sqrt{\left(\nabla^T u\,\hat{n}(s)\right)^2+\left(\nabla^T w\,\hat{n}(s)\right)^2}$$

Equivalently to the displacement $du\hat{\imath}+dw\hat{\jmath}$ one can define a displacement $\left(d\tilde{u}+\partial_s\tilde{w}\right)\hat{l}(s)+\partial_\delta\tilde{w}\hat{n}(s)$ with the functions $\tilde{u}$ and $\tilde{w}$ with correspondence to u and w given by the expressions $\nabla\tilde{u}=\hat{l}(s)\sqrt{\left(\nabla^T u\,\hat{l}(s)\right)^2+\left(\nabla^T w\,\hat{l}(s)\right)^2}$ ,

$\nabla\tilde{w}=\hat{n}(s)\sqrt{\left(\nabla^T u\,\hat{n}(s)\right)^2+\left(\nabla^T w\,\hat{n}(s)\right)^2}$ .

Then the differential deformation is written

$$\left(d\tilde{u}+\partial_s\tilde{w}\right)\hat{l}(t)+\partial_\delta\tilde{w}\,\hat{n}(t)=\left(\left\|\nabla\tilde{u}\right\|+\tilde{w}\hat{l}^{\,T}(s)\frac{d\hat{n}(s)}{ds}\right)ds\,\hat{l}(t)+\left\|\nabla\tilde{w}\right\|d\delta\,\hat{n}(t)$$

(1). But $\dfrac{d\hat{n}(s)}{ds}=\dfrac{H(\tilde{w})-I\tilde{w}_{nn}}{\left\|\nabla\tilde{w}\right\|}\hat{l}(s)=\dot{\phi}\,\hat{l}(s)$ (2).

Then $\tilde{u}$ and $\tilde{w}$ are given by the differential equations

$$\frac{\partial\tilde{w}}{\partial\delta}=\left\|\nabla\tilde{w}\right\|\ (3)\qquad \frac{\partial\tilde{w}}{\partial s}=-\tilde{w}\frac{\tilde{w}_{nn}}{\left\|\nabla\tilde{w}\right\|}\ (4)\qquad \frac{\partial\tilde{u}}{\partial s}=\left\|\nabla\tilde{u}\right\|\ (5)$$

Strains $\varepsilon_{ll},\varepsilon_{nn},\varepsilon_{ln}$ and $\varepsilon_{nl}$ caused by the deformation functions $\tilde{u}$, $\tilde{w}$ are given by the following expressions:

$$\varepsilon_{ll}=\left\|\nabla\tilde{u}\right\|-1\qquad \varepsilon_{nn}=\left\|\nabla\tilde{w}\right\|-1\qquad \varepsilon_{nl}=\varepsilon_{ln}=-\frac{1}{2}\left(\tilde{w}-\delta_0\right)\frac{\tilde{w}_{nn}}{\left\|\nabla\tilde{w}\right\|}$$

According to the assumption of elastic deformation, the expression connecting stresses and strains along $\hat{l}(s)$, $\hat{n}(s)$ is expressed via the relation $\tilde{\sigma}=\tilde{\mathrm{E}}\tilde{\varepsilon}$ ; where $\tilde{\mathrm{E}}=\begin{bmatrix}E_{11} & E_{12}\\ E_{21} & E_{22}\end{bmatrix}$ a constant matrix.

### C. Solutions of deformation functions' PDEs via morphological operations

For an arbitrary point (x,y) we consider the definitions of A) its initial distance from a point Σ of the symmetry line suffering s-deformation obtained via

$$\left\{\delta_0(x,y)\right\}(s)=\min_\tau\left\{\sqrt{\left(x-x_\mu(\tau)\right)^2+\left(y-y_\mu(\tau)\right)^2}\right\}\quad (6)$$

B) the correspondence of Σ with a unique Σ' of the undeformed symmetry line suffering δ-deformation obtained via $\left\{s_0(x,y)\right\}(\delta)=\arg\min_\tau\left\{\left(x-x_\mu(\tau)\right)^2+\left(y-y_\mu(\tau)\right)^2\right\}$ (7)

Then PDE (3) with initial condition $\left\{\delta_0(x,y)\right\}(s)$ is equivalent to the action over $\left\{\delta_0(x,y)\right\}(s)$ of a dilation filter at scale s with a flat disk kernel [7]. Namely

$$\tilde{w}(s,\delta)=M^+\left[\left\{\delta_0(x,y)\right\}(s)\right](\delta)=\sup_{\|\vec{\varepsilon}\|\le\delta}\left\{\left\{\delta_0\left((x,y)+\vec{\varepsilon}\right)\right\}(s)\right\}\quad (8)$$

Similarly PDE (5) with initial condition $\left\{s_0(x,y)\right\}(\delta)$ is equivalent to the dilation of $\left\{s_0(x,y)\right\}(\delta)$ with flat disk kernel at scale s

$$\tilde{u}(s,\delta)=M^+\left[\left\{s_0(x,y)\right\}(\delta)\right](s)=\sup_{\|\vec{\varepsilon}\|\le s}\left\{\left\{s_0\left((x,y)+\vec{\varepsilon}\right)\right\}(\delta)\right\}\quad (9)$$

For the solution of (4), first we express the directional derivative of $\tilde{w}_n$ at an arbitrary direction $\hat{v}$, $\tilde{w}_{nv}=\hat{v}^T H(\tilde{w})\hat{n}=\tilde{w}_{nl}\hat{v}^T\hat{l}+\tilde{w}_{nn}\hat{v}^T\hat{n}$ (10).

But, performing dot product of (2) with $\hat{n}$ results $\tilde{w}_{nl}=0$. By substituting in (10) we obtain $\tilde{w}_{nv}=\tilde{w}_{nn}\hat{v}^T\hat{n}$. This relation bounds $\tilde{w}_{nv}$ and hence $\dfrac{\tilde{w}_{nv}}{\left\|\nabla\tilde{w}\right\|}=\dfrac{\partial}{\partial v}\left(\ln\left\|\nabla\tilde{w}\right\|\right)$ .

Hence (4) is written $\dfrac{\partial}{\partial s}\ln\tilde{w}=-\dfrac{\partial}{\partial n}\left(\ln\left\|\nabla\tilde{w}\right\|\right)$ with initial conditions $\left\{\tilde{w}(x,y)\right\}(0,\delta)=M^+\left[\delta_0(x,y)\right](\delta)$ and $\left\{\tilde{\phi}_0(x,y)\right\}(0,\delta)=\ln\left(\left\|\nabla\tilde{w}\right\|\right)(0,\delta)$. Writing $-\dfrac{\partial}{\partial n}\left(\ln\left\|\nabla\tilde{w}\right\|\right)$ as an extreme of $\dfrac{\partial}{\partial v}\left(\ln\left\|\nabla\tilde{w}\right\|\right)$ one obtains:

$$\frac{\partial}{\partial s}\ln\tilde{w}=\begin{cases}\dfrac{\partial}{\partial s}M^+\left[\left\{\tilde{\phi}_0(x,y)\right\}(0,\delta)\right](s) & \dfrac{d}{ds_0(\delta)}\phi(s_0(\delta))<0\\[2ex] \dfrac{\partial}{\partial s}M^-\left[\left\{\tilde{\phi}_0(x,y)\right\}(0,\delta)\right](s) & \dfrac{d}{ds_0(\delta)}\phi(s_0(\delta))>0\end{cases}\quad (11)$$

where $s_0(\delta)$ is given for δ-deformation using (7) and the initial condition $\left\{\tilde{\phi}_0(x,y)\right\}(0,\delta)$ can be derived straight from a dilated version of the global initial conditions $(s_0,\delta_0)$.

To unify both these cases in one process we define the

function $\{\kappa_\varphi(x,y)\}(s_0(\delta)) = -(\operatorname{sgn}\dot{\phi}(s_0(\delta)))\infty$. Then we adopt the process

$$\alpha[g(\delta)](s) = \sup[M^-[g(\delta)](s), \inf[M^+[g(\delta)](s), \kappa_\phi(s_0(\delta))]]$$

(12). This functional's derivative is given by the formula

$$\frac{\partial}{\partial\sigma}\alpha[g(\delta)](\sigma) = \begin{cases} \frac{\partial}{\partial\sigma}M^+[g(\delta)](\sigma) & \kappa_\varphi(s_0(\delta)) < M^+[g(\delta)](\sigma) \Leftrightarrow \frac{d\phi(s_0(\delta))}{ds_0(\delta)} < 0 \\ \frac{\partial}{\partial\sigma}M^-[g(\delta)](\sigma) & \kappa_\varphi(s_0(\delta)) > M^+[g(\delta)](\sigma) \Leftrightarrow \frac{d\phi(s_0(\delta))}{ds_0(\delta)} > 0 \end{cases}$$

Letting $g(\delta) = \{\tilde{\phi}_0(x,y)\}(0,\delta)$ the above filter on s-scale space gives a solution for (11) and equivalently of (4). Finally, correspondence between (4) with initial conditions $g(\delta)$ and filter $\alpha[g(\delta)](s)$, gives

$$\{\tilde{w}(x,y)\}(s,\delta) = \{\tilde{w}(x,y)\}(0,\delta)\exp\left(a\left[\{\tilde{\phi}_0(x,y)\}(0,\delta)\right](s)\right) \quad (13)$$

## III. Image Analysis for the Determination of the Deformed Body Neutral Line

### A. Confirmation that the neutral line passes from the middle of its cross sections

Consider a section A normal to the symmetry line in the undeformed object's state. Then, the vertical shear force V and force $N$ normal to $A$ and along the symmetry line are given by the expressions:

$$V = \oint_A \sigma_{ln} dA \quad (14) \qquad \text{and} \qquad N = \oint_A \sigma_{ll} dA \quad (15)$$

We assume that the object is in an equilibrium position each time a photograph is taken. Then, equilibrium along symmetry line implies that $N = 0$, $V = 0$. Since we have adopted the assumption that the generalized Hooke's law holds, it follows that

$$N = E_{11}\left(\|\nabla\tilde{u}\| - 1\right)A - E_{12}\frac{1}{2}\frac{\tilde{w}_{nn}}{\|\nabla\tilde{w}\|}\oint_A(\tilde{w} - \delta_0)dA = E_{11}\left(\|\nabla\tilde{u}\| - 1\right)A \quad (16)$$

Combining (16) and $N = 0$, we deduce that $\{\tilde{s}(x,y)\}(\delta) = s_0 + s$ (17) indicating that s-deformation is only offsetting the length of the initial symmetry line and hence that it can be ignored. Now, symmetry line's stresses in the direction tangent to it, $\sigma_{ll}$, are given via

$$\sigma_{ll} = -\frac{E_{12}}{2}(\tilde{w} - \delta_0)\frac{\tilde{w}_{nn}}{\|\nabla\tilde{w}\|} \quad (18)$$

$$V = E_{12}\oint_A\left(\|\nabla\tilde{w}\| - 1\right)dA - \frac{E_{11}}{2}\frac{\tilde{w}_{nn}}{\|\nabla\tilde{w}\|}\oint_A(\tilde{w} - \delta_0)dA = E_{12}\oint_A\left(\|\nabla\tilde{w}\| - 1\right)dA \quad (19)$$

Combining (19) and $V = 0$, we deduce that $\{\tilde{\delta}(x,y)\}(\delta) = \delta_0 + \delta$ (20), which similarly results that δ-deformation is only offsetting the distances from the undeformed symmetry line and hence that it can be ignored. Now, symmetry line's stresses in the directions normal to it, are given via $\sigma_{ln} = -\frac{E_{11}}{2}\frac{\tilde{w}_{nn}}{\|\nabla\tilde{w}\|}(\tilde{w} - \delta_0)$ (21).

Combining (21) and (18) with zero offsetting of $\delta_0(x,y)$ we obtain

$$\sigma_{ll} = -\frac{E_{12}}{2}\{\tilde{\phi}(x,y)\}(s)\delta_0\frac{\tilde{w}_{nn}}{\|\nabla\tilde{w}\|},\ \sigma_{ln} = -\frac{E_{11}}{2}\{\tilde{\phi}(x,y)\}(s)\delta_0\frac{\tilde{w}_{nn}}{\|\nabla\tilde{w}\|}$$

To study the stress that symmetry line suffers we let $\delta_0 \to 0$ then

$$\{\tilde{\phi}_0(x,y)\}(\delta) = \lim_{\delta_0\to 0}\ln\left(\frac{\partial}{\partial n}\delta_0(x,y)\right) = 0 \Rightarrow \lim_{\delta_0\to 0}\{\tilde{\phi}(x,y)\}(s) = 1$$

and finally (13) results

$$\lim_{\delta_0\to 0}\{\tilde{w}(x,y)\}(s,\delta) = \lim_{\delta_0\to 0}\delta_0\{\tilde{\phi}(x,y)\}(s) = 0.$$

Therefore, the curve to which symmetry line is transformed suffers no stress; the curve formed by all these unstressed points, usually called the neutral line, has the following properties:

a) It is the curve to which the symmetry line is transformed due to the elastic deformation process.

b) No stress is exerted along it.

c) As a consequence, the neutral line and the body symmetry line are of the same length.

d) The neutral line passes from the middle point of each cross section in the 2D image representation of the deformed body.

e) The undeformed cross sections, initially perpendicular to the symmetry line, remain perpendicular to the neutral line even after the body's deformation.

### B. An important property of the deformed object contour tangents

In this paragraph we will state a new lemma, that has been proved by the authors, in order to deal with the problem of spotting deformed body's cross sections.

*Lemma*

Let $\Sigma_1\Sigma_2$ be the symmetry line of the unwrapped body and $AD$ an arbitrary cross section, intersecting $\Sigma_1\Sigma_2$ at point $M$ where part $\Sigma_1 M$ of the symmetry line has length s. Then, due to the deformation, $AD$ moves to a section $A'D'$, perpendicular to the neutral line at point $M'$. Let moreover U' and L' be the upper and lower boundary curves of the deformed body, respectively and $N'$ be its neutral line. If $\vec{T}_{A'}^{U'}$ is the tangent vector of $U'$ at $A'$, $\vec{T}_{D'}^{L'}$ the tangent vector of $L'$ at $D'$ and $\vec{L}_{M'}$ is the tangent vector of the deformed symmetry line at point $M'$; then it holds that $\angle\left(\overrightarrow{A'D'}, \vec{T}_{A'}^{U'} - \vec{L}_{M'}\right) + \angle\left(\overrightarrow{A'D'}, \vec{T}_{D'}^{L'} - \vec{L}_{M'}\right) = \pi$.

### C. Object contour extraction and its polynomial approximation

As the introduced methodology makes use of the border line of each parasite, it is necessary to obtain well-defined boundary lines of all instances of the examined parasites. In order to achieve this, the following method is used:

First, we have applied various image segmentation methods ([8],[9]) in order to obtain quite clear-cut and accurate region borders of each parasite. A rather simple

method that seems to work well is the one that uses each parasite's pixel intensity histogram and the lower turning point of it. All pixels with intensity lower than this turning point may be considered to belong to the parasite body. This method may generate various artifacts that may be removed by application of proper morphological filters, see e.g. [10].

As it will become evident from the subsequent analysis, in order that the introduced methodology is applied, each contour line must have the following properties: A) each pixel must have exactly two neighboring pixels B) no isolated pixels or groups of pixels are allowed and C) three pixels must not form a compact right ( $90^\circ$ ) angle. Since no edge detection algorithm can generate the parasite contour in this form, suitable software has been developed to achieve that.

The next step is to determine if there are specific mathematical curves that optimally fit the object body, e.g. a parasite, contour in the obtained images. There are various techniques for achieving this goal (e.g. [11],[12]). For the present application the following method proved quiet satisfactory:

The curve parameter is chosen to be its contour length s, calculated via the distance of the successive pixels that form it. Subsequently, we approximate the variables x and y of the body contour by polynomials up to 21 degree:

$$\begin{aligned} x(s) &= a_n s^n + a_{n-1} s^{n-1} + a_{n-2} s^{n-2} + ... + a_1 s^1 + a_0 \\ y(s) &= b_n s^n + b_{n-1} s^{n-1} + b_{n-2} s^{n-2} + ... + b_1 s^1 + b_0 \end{aligned} \quad (22)$$

Let $\overrightarrow{r_i^B}$, $i = 1,2,...,N^B$ be the centers of the pixels forming the upper contour and let $\Pi = \{a_n, a_{n-1},..., a_1, a_0, b_n, b_{n-1},..., b_1, b_0\}$. Hence the parametric vector equation of the prototype curve is $\overrightarrow{r^M}(s \mid \Pi) = x(s)\vec{i} + y(s)\vec{j}$.

Next, we compute the optimal set of parameters $\Pi^O$ and the corresponding sequence of values of the independent variable $s_i$, $i = 1,2,...,N^B$, so that $\overrightarrow{r^M}(s_i \mid \Pi^O)$ best fits $\overrightarrow{r_i^B}$ according to the chosen quadratic norm $E_2 = \sum_{i=1}^{N^B} \left| \overrightarrow{r_i^B} - \overrightarrow{r_i^M} \right|^2$. This minimization has been performed by usage of the Nelder – Mead method [13] starting from a tentative initial position $\Pi^1$ and each time generating a new set of parameter values $\Pi^2, \Pi^3$, etc, so that $E_2$ eventually converges to its minimum value, in which case the optimal set of parameters $\Pi^O$ is obtained.

### *D. Determining deformed body's neutral line via image processing*

In this section, we will analytically describe the methodology we have introduced and applied for determining the exact position of the neutral line in the deformed body image, as well as the positions of the cross sections that, by hypothesis, always remain undeformed and normal to the neutral line. The application of this methodology has been made on the available parasite images and comprises the following steps:

*Step1:* We, first, extract the parasite contour. Next, we spot the head and the tail of the parasite as follows: First, to spot the tail, for each contour pixel p we consider the sets of pixels $P_L$ that lie on its left and $P_R$ that lie on its right. We approximate both $P_L$ and $P_R$ with line segments in the Least Squares sense. We let the tail T be the pixel where these two line segments form the most acute angle.

Second, we spot the parasite "head" H: We move away from the tail and we locally approximate the contour by polynomials of fifth degree, of which we compute the curvature. We let the "head" be the point of maximum curvature, which also lies between 0.4 and 0.6 of the whole contour length.

*Step2:* We divide the whole contour into two parts I and II (arbitrarily called upper and lower), that both end at the parasite "head" and "tail". Then we approximate both parts with polynomials of type (22). All performed experiments indicate that this approximation is excellent. We form a dense sequence $M_j^{II}$, $j = 1...N^{II}$ of points belonging to the polynomial curve best fitting part II and a less dense sequence $M_i^I$, $i = 1...N^I$ on curve fitting part I; let $\vec{\tau}_i^I$ and $\vec{\tau}_j^{II}$ be the unit tangent vectors to these model curves at each $M_i^I$ and $M_j^{II}$ respectively.

*Step3:* Subsequently, we spot parasite's neutral line by applying the aforementioned lemma and the results of paragraphs A and B as follows:

We move away from tail T along part I and we connect $M_1^I$ with each point of set $M_j^{II}$, $j = 1...K$, where K is a predefined number of pixels, say 5% of the whole contour length. We form vectors $\vec{r}_{1,j} = \overrightarrow{M_j^{II} M_1^I}$, $j = 1,...,K$. We keep only those vectors $\vec{r}_{1,j}$ that lie entirely within the parasite body and for these we compute the angles $\varphi_{1,j}^I$ and $\varphi_{1,j}^{II}$ formed by each vector $\vec{r}_{1,j}$ and the tangent vectors $\vec{\tau}_1^I$ and $\vec{\tau}_{1,j}^{II}$ respectively. Then, we define the sequence $\Delta\varphi_{1,j} = \left| \varphi_{1,j}^I + \varphi_{1,j}^{II} - \pi \right|$ and we let $N_1^{II}$ be that point where the minimum value of the sequence $\Delta\varphi_{1,j}$ occurs, say the $d_1$-th of sequence $M_j^{II}$; we consequently define $\overrightarrow{M_1^I N_1^{II}}$ to be a cross section of the parasite that remains undeformed and normal to the neutral line.

Next we compute the second cross section as follows: We move away from the tail vertex T and $M_1^I$ at $M_2^I$ and once more, we define the set of points $M_{d_1+j}^{II}$, $j = 1,...,K$. Proceeding as before we define vectors, $\vec{r}_{2,j} = \overrightarrow{M_{d_1+j}^{II} M_2^I}$, $j = 1,...,K$. We compute the corresponding angles $\varphi_{2,j}^I$ between $\vec{r}_{2,j}$ and $\vec{\tau}_2^I$, as well as $\varphi_{2,j}^{II}$ between $\vec{r}_{2,j}$ and $\vec{\tau}_{d_1+j}^{II}$. We spot the minimum of the sequence $\Delta\varphi_{2,j} = \left| \varphi_{2,j}^I + \varphi_{2,j}^{II} - \pi \right|$, which occurs at point $N_2^{II}$, say the $d_2$-th point of sequence $M_j^{II}$. We let $\overrightarrow{M_2^I N_2^{II}}$ be

the second cross section that remains undeformed and normal to the neutral line.

Finally we proceed in obtaining all cross sections $\overrightarrow{M_i^I N_i^{II}}$ passing from $M_i^I$, $i=1...N^I$ by the same method (Figures 1A,B). The middle point of these cross sections belongs to the neutral line and the unit vector normal to these sections is tangent to the neutral line.

## IV. Image Operations to Unwrap the Deformed Body

We have shown in Section III that under the adopted assumptions the neutral line undertakes no stress and it is found in the middle of the corresponding cross section. Consequently, we define the neutral line of the deformed parasite to be the locus of the middle points $K_\nu$ of the cross sections $M_\nu^I N_\nu^{II}$ as they are determined above. We achieve unwrapping of the deformed body by means of a new method consisting of the following steps:

*Step 1:* Initially, the vector parametric equation of the neutral line is approximated via 21th degree polynomials of type (4.3.1) that best fit points $K_\nu$ in the least squares sense, thus obtaining $\vec{r}_\mu(s)=\left(x_\mu(s),y_\mu(s)\right)$. Using this vector parametric equation, we compute the unit directional vectors along $\vec{r}_\mu(s)$, $\hat{l}(s)=\dfrac{\dot{x}_\mu(s)\hat{i}+\dot{y}_\mu(s)\hat{j}}{\sqrt{\dot{x}_\mu(s)^2+\dot{y}_\mu(s)^2}}$, $\hat{n}(s)=\dfrac{-\dot{y}_\mu(s)\hat{i}+\dot{x}_\mu(s)\hat{j}}{\sqrt{\dot{x}_\mu(s)^2+\dot{y}_\mu(s)^2}}$, as well as the curvature $c(s)=\dfrac{\dot{x}_\mu\ddot{y}_\mu-\ddot{x}_\mu\dot{y}_\mu}{\dot{x}_\mu{}^2+\dot{y}_\mu{}^2}$.

*Step 2:* Afterwards, at any pixel point $(x,y)$, inside the deformed body, we attribute the values the following two images, $s_0(x,y)$, $\delta_0(x,y)$, have at this point

$$\delta_0(x,y)=\min_s\left\{\sqrt{\left(x-x_\mu(s)\right)^2+\left(y-y_\mu(s)\right)^2}\right\}$$

$$s_0(x,y)=\arg\min_s\left\{\sqrt{\left(x-x_\mu(s)\right)^2+\left(y-y_\mu(s)\right)^2}\right\}$$

These two images play the role of initial conditions for the PDEs (3), (5), (4) which describe the deformation functionals $\{\tilde{\delta}(x,y)\}(\delta)$, $\{\tilde{s}(x,y)\}(s)$, $\{\tilde{\phi}(x,y)\}(s)$ respectively.

*Step 3:* We have proved that the solution of deformation differential equations is equivalent to applying to $s_0(x,y)$, $\delta_0(x,y)$ dilations (5) and 3) respectively, and the filter $a[g,\kappa](s)$ to the dilated $\delta_0(x,y)$ as formula (4) indicates. As it was shown, the crucial operation is curvature deformation $\{\tilde{\phi}(x,y)\}(s)$ given by formula (13). Namely $\{\tilde{\phi}(x,y)\}(s)=\exp(\alpha[g,\kappa_\phi](s))$, where $\kappa_\phi(x,y)=-\mathrm{sgn}(c(x,y))\infty$, $g(x,y)=\ln\tilde{\phi}_0(x,y)$ and $\tilde{\phi}_0(x,y)=\|\nabla\delta_0(x,y)\|$. This image represents, through scale s, all curvature deformations implied on the body. Since we want to straighten parasite bodies we demand zero curvature of symmetry line. For each pixel $(x,y)$ in the deformed parasite body, we determine the proper scale $\sigma(x,y)$ that minimizes $\{\tilde{\phi}(x,y)\}(\sigma)$, namely $\sigma(x,y)=\arg\min_s\left\{\left|\{\tilde{\phi}(x,y)\}(s)\right|\right\}$. Thus, if the given image of the deformed body is $f(x,y)$, then the above procedure generates an image that corresponds to the unwrapped body described by $f_T(\sigma(x,y),\delta_0(x,y))=f(x,y)$.

## V. Evaluation of the Introduced Methodology-Conclusion

### A. Evaluation of the method of unwrapping the deformed bodies

If the assumptions made in this paper and the introduced methodology are correct, one expects that different instances of a specific body deformation will generate the same undeformed contour of the body, at least with an acceptable approximation. In particular, for the application in hand, one expects that different images of the deformed parasite must offer quiet close unwrapped versions after application of the methodology introduced in sections III and IV. In fact, the undeformed parasite borders have a difference that might be considered negligible in respect to the parasite dimensions. We have employed five different measures to describe the differences between the shapes of the unwrapped parasite that resulted from different phases. These measures are :

1) $a_{1,i}=\dfrac{\left(\ell_i^P-\overline{\ell}^P\right)}{\overline{\ell}^P}\cdot 100\%$, where $\ell_i^P$ is the length of the unwrapped parasite obtained from the ith wrapped larva phase and $\overline{\ell}^P$ its mean value. 2) $a_{2,i}=\dfrac{\left(E_i^P-\overline{E}^P\right)}{\overline{E}^P}\cdot 100\%$, where $E_i^P$ is the area of the unwrapped parasite. 3) $a_{3,i}=\dfrac{mean_j\left(y_{i,j}-\bar{y}_j\right)}{mean_j\left(\bar{y}_j\right)}\cdot 100\%$, where $y_{i,j}$ is the width of the unwrapped at point $x_j$; hence, we define $\bar{y}_j=mean_i\left(y_{i,j}\right)$. 4) $a_{4,i}=\dfrac{\left(\Pi_i^P-\overline{\Pi}^P\right)}{\overline{\Pi}^P}\cdot 100\%$, where $\Pi_i^P$ is the perimeter of the unwrapped parasite. 5) $a_{5,i}=\dfrac{\left(C_i^P-\overline{C}^P\right)}{\overline{C}^P}\cdot 100\%$, where $C_i^P$ is the maximum cross section diameter of the unwrapped parasite.

The mean value and standard deviation of quantities $a_{1,i}$, $a_{2,i}$, $a_{3,i}$, $a_{4,i}$, $a_{5,i}$ are shown in Table I. Evidently, the introduced method for deducing the undeformed body version from its deformation images, seems consistent, reliable and robust.

### B. Conclusion

In this paper, a new methodology has been introduced that exploits images of elastic body deformation instances, so as to verify assumptions about its mechano-elastic properties. The validity of these assumptions allows for unwrapping the body, i.e. for obtaining the body undeformed version from its deformed image. We have reformulated some fundamental relations from Elasticity Theory, in order to derive equations

for the 2D body deformation, which can be subsequently interpreted as a set of morphological operations acting on a 2D body image. By applying the inverse morphological operation we obtain the undeformed image of the body via the process described in Section IV.

Application of this methodology to 193 images of highly deformed parasites of domestic animals, offered straightened contours and body versions that seem to be consistent and reliable representations of the undeformed parasites. Employing these unwrapped parasite versions, a very successful automatic recognition of parasites from their images have been achieved.

## REFERENCES


[1] Richard L. Ehman and James F. Greenleaf, "Reconstruction of Elasticity and Attenuation Maps in Shear Wave Imaging: An Inverse Approach", *Medical Image Computing and Computer-Assisted Intervention — MICCAI'98*, vol. 1496, Lecture Notes in Computer Science, Springer Berlin / Heidelberg, p. 606-613, 1998.

[2] Theodoropoulos, G., Loumos, V., Anagnostopoulos, C., Kayafas, E., & Martinez-Gonzales, B., A digital image analysis and neural network based system for identification of third-stage parasitic strongyle larvae from domestic animals, *Computer Methods and Programs in Biomedicine*, v. 62, no. 2, p. 69-76, 2000.

[3] X. Pennec, R. Stefanescu, V. Arsigny, P. Fillard, and N. Ayache, "Riemannian Elasticity: A Statistical Regularization Framework for Non-linear Registration", *Medical Image Computing and Computer-Assisted Intervention — MICCAI 2005*, vol. 3750, Lecture Notes in Computer Science, Springer Berlin / Heidelberg, p. 943-950, 2005.

[4] Alain Trouve, "Diffeomorphisms Groups and Pattern Matching in Image Analysis", *International Journal of Computer Vision*, vol. 28(3), Kluwer Academic Publishers, Netherlands, 1998, p.213-221

[5] Christensen, G.E. Rabbitt, R.D. and Miller, M.I., "Deformable templates using large deformation kinematics", *IEEE Transactions on Image Processing,* vol. 5, no. 10, p. 1435-1447, 1996.

[6] Demetri Terzopoulos, Andrew Witkin and Michael Kass, "Symmetry-Seeking models and 3D object reconstruction", *International Journal of Computer Vision*, vol. 1, no. 3, Springer Netherlands, p. 211-221 1988.

[7] Roger W. Brockett and Petros Maragos, "Evolution Equations for Continuous-Scale Morphological Filtering", *IEEE Transactions on Signal Processing*, vol. 42, no. 12, p. 3377-3386, 1994

[8] Adam, Gillian, Xiaoyi, Patrick J., Horst, Dmitry B., Kevin, David W., Andrew, Robert B., "An Experimental Comparison of Range Image Segmentation Algorithms", *IEEE Transactions on PAMI*, vol. 18, no. 7, p. 673-689, 1996.

[9] Lee, D., Baek, S., & Sung, K. (1997). Modified k-means Algorithm for Vector Quantizer Design, *IEEE Signal Processing Letters*, Vol. 4, No. 1, pp2-4.

[10] Panagopoulos Th., Papaodysseus C., Exarhos M., Triantafillou C., Roussopoulos G. & Roussopoulos P. (2004). Prehistoric Wall-Paintings Reconstruction Using Image Pattern Analysis And Curve Fitting, *WSEAS Transactions on Electronics 1*, no 1 pp. 108-113.

[11] Papaodysseus, C., Exarhos, M., Panagopoulos, Th., Triantafillou, C., Roussopoulos, G., Pantazi, Af., Loumos, V., Fragoulis & D., Doumas, C. (2005). Identification of Geometrical Shapes in Paintings and its Application to Demonstrate the Foundations of Geometry in 1650 BC. *IEEE Transactions on Image Processing*, Vol. 14, No. 7, p. 862-873.

[12] Ahn, S.J., Rauh, W., Cho, H.S., and Warnecke, H.J., "Orthogonal Distance Fitting of Implicit Curves and Surfaces", *IEEE Transactions on PAMI*, p. 620-638 2002.

[13] J.A. Nelder and R. Mead, "A Simplex Method for Function Minimization", *Computer Journal*, vol.7, p. 308-313 1965


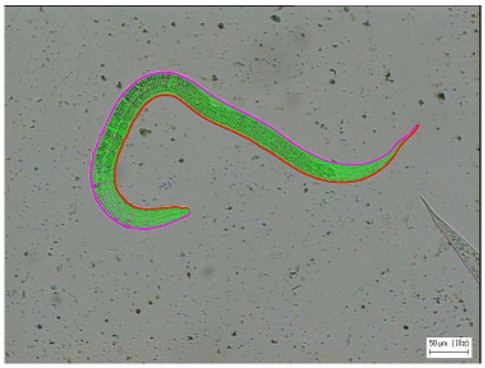

Figure 1A. Determination of the cross sections in a highly deformed parasite image. A first example.

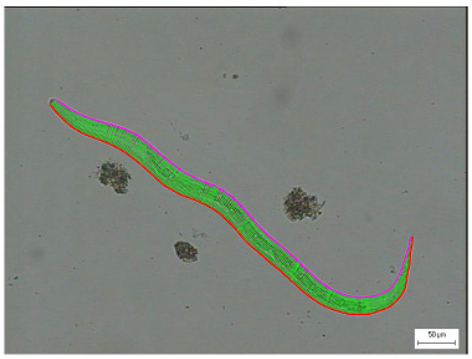

Figure 1B. Another example of cross sections determination

Fig. 2A. Generating the unwrapped version of the parasite of Fig. 1A

Fig. 2B. Generating the unwrapped version of the parasite of Fig. 1B

**Table I**

| | Evaluation the discrepancy between the unwrapped versions of Figure 1A. | | Evaluation the discrepancy between the unwrapped versions of Figure 1B. | | Average discrepancy of all experimental results | |
|---|---|---|---|---|---|---|
| | Mean value | Standard Deviation | Mean value | Standard Deviation | Mean value | Standard Deviation |
| $a_1$ (Length): | 0.82 | 0.29 | 1.04 | 0.73 | 0.91 | 0.56 |
| $a_2$ (Area): | 2.30 | 1.18 | 1.41 | 0.62 | 1.73 | 1.01 |
| $a_3$ (Width): | 1.87 | 1.06 | 1.32 | 0.60 | 1.68 | 0.94 |
| $a_4$ (Perimeter): | 0.84 | 0.34 | 1.07 | 0.74 | 0.95 | 0.59 |
| $a_5$ (Max cross section diameter): | 2.63 | 1.68 | 2.62 | 1.63 | 2.71 | 1.72 |